Study of Mg-Fe content in tourmalines from the dravite-schorl series by Raman spectroscopy

Lorenzo Pasetti[1], Laura Fornasini[1], Luciana Mantovani[2], Sergio Andò[3], Simona Raneri[4], Vincenzo Palleschi[4], Danilo Bersani[1]

[1] *Department of Mathematical, Physical and Computer Sciences, University of Parma, Parco Area delle Scienze 7/A, 43124 Parma, Italy*
[2] *Department of Chemistry, Life Sciences and Environmental Sustainability, University of Parma, Parco Area delle Scienze 157/A, 43124 Parma, Italy.*
[3] *Laboratory for Provenance Studies, Department of Earth and Environmental Sciences, University of Milano-Bicocca, Piazza della Scienza 4, 20126, Milan, Italy.*
[4] *Applied and Laser Spectroscopy Laboratory, Institute of Chemistry of Organometallic Compounds, National Research Council, CNR Research Area, Pisa, Italy*

Abstract

Thanks to their high chemical and mechanical stability, their diffusion in all types of detrital sediments, and their complex structural formula ($XY_3Z_6(T_6O_{18})(BO_3)_3V_3W$), tourmalines have attracted strong interest in provenance studies since, from their chemical composition, it is possible to reconstruct the source rocks in ancient sediments.

Dravite and schorl, belonging to the alkali-subgroup 1, are the most abundant tourmaline species, and they have different Y-site compositions in the unit cell: dravite has more magnesium, while schorl has a higher iron content. For this reason, it is important to measure the Mg-Fe relative content in order to classify the analysed tourmalines in the dravite-schorl series.

Raman spectroscopy is a suitable technique as it allows quick and easy measurements that provide chemical and structural information on tourmalines with a high spatial resolution, thus allowing analysis of small grains that could be found in sediments.

In this work, we correlated the relative Mg-Fe content (x=Mg/(Mg+Fe)) in different tourmaline samples from the dravite-schorl series ($Na(Mg_xFe_{1-x})_3Al_6(Si_6O_{18})(BO_3)_3(OH)_3OH$) with variations in Raman spectrum parameters in order to find a model for quick tourmaline identification useful for provenance studies.

The chemical compositions of the analysed tourmalines are obtained by SEM-EDS (Scanning Electron Microscope coupled with Energy Dispersive Spectroscopy).

Raman measurements with a portable spectrometer have also been performed in order to evaluate our results for *in-situ* applications.

Keywords: Tourmaline, Dravite, Schorl, Chemical composition.

Introduction

Tourmalines are a borosilicate mineral supergroup with a complex chemical composition represented by the formula $XY_3Z_6(T_6O_{18})(BO_3)_3V_3W$, in which each crystal site could be occupied by the following elements [1,2]:

X site: Na^+, Ca^{2+}, □ *(vacant site),* K^+.

Y site: $Fe^{2+}, Mg^{2+}, Mn^{2+}, Al^{3+}, Li^+, Fe^{3+}, Cr^{3+}, Ti^{4+}, Zn^{2+}, Cu^{2+}, V^{3+}$.

Z site: $Al^{3+}, Fe^{3+}, Mg^{2+}, Fe^{2+}, Cr^{3+}, V^{3+}$.

T site: Si^{4+}, Al^{3+}, B^{3+}.

B site: B^{3+}.

V site: $(OH)^-, O^{2-}$.

W site: $F^-, (OH)^-, O^{2-}$.

Tourmalines have a wide stability range at different temperatures (up to 725–950 °C depending on pressure) and pressure conditions (under 7 GPa) [3,4], which allows them to be present in almost all geological settings with a high spread in all types of detrital sediments [5]. Moreover, they can keep track of the elements taking part in crystal growth processes thanks to their high mechanical and chemical stability [6,7]. These properties make tourmalines suitable for provenance studies, as their composition can be used as an indicator to reconstruct the possible source-rocks in ancient sediments [8–13].

Micro-Raman spectroscopy can be a suitable technique to investigate tourmaline grain composition in sediments as it allows quick measurements with a high spatial resolution, but a model to recognise different tourmaline species and retrieve information on their chemical composition from Raman spectrum parameters needs to be developed.

Many tourmaline groups and subgroups could be identified from their composition, and more than thirty-three distinct species have been found [7]. In this work, we focused on two species belonging to alkali-subgroup1 [1], dravite and schorl, which are represented by the end member formulas $NaMg_3Al_6(Si_6O_{18})(BO_3)_3(OH)_3OH$ and $NaFe_3Al_6(Si_6O_{18})(BO_3)_3(OH)_3OH$, respectively, and which are the most diffused tourmaline species. The alkali-group is characterised by the X site being mainly occupied by Na^+or, more rarely, by K^+, while the main difference between these two species is the Y site's occupation: in dravite, characterised by a pale brown to

brownish black colour, we have a higher Mg^{2+} content, whereas in schorl, typically bluish-black to black, there's more Fe^{2+}. Between the two end members, there are all the intermediate compositions with different magnesium-iron relative content in Y sites, which form the dravite-schorl series, represented by the formula $Na(Mg_xFe_{1-x})_3Al_6(Si_6O_{18})(BO_3)_3(OH)_3OH$, where x indicates the relative magnesium-iron content (x = Mg/(Mg+Fe)). The various compositions reflect the composition of the host magma where tourmaline first nucleated; in fact, differing magnesium and iron relative contents are connected to crystal development conditions in the magma [4].

The complexity of tourmalines structure and composition makes their study non-trivial; for this reason, we want to focus only on these two species and on their magnesium and iron content (Mg/(Mg+Fe)) in order to limit the complexity of the model to be implemented and lay solid foundations for future developments.

The main peaks of the Raman spectrum of tourmaline are located in two regions: the so-called fingerprint region between 150 and 750 cm^{-1} [14,15] and the stretching region of the OH groups between 3400 and 3800 cm^{-1} [16]. In the lower part of the spectrum, several subregions can be identified where vibrational modes associated with different crystallographic sites of the unit cell are present. Between 200 and 315 cm^{-1}, the vibrational modes of the YO_6 octahedra are present, represented by three main peaks called P_1, P_2, and P_3. In the range of 360-375 cm^{-1}, we have peaks corresponding to the vibrational modes of the ZO_6 octahedra, among which the one with the highest intensity is indicated as P_Z. Finally, in the region between 600 and 750 cm^{-1}, the vibrational modes of the bridging oxygen atoms in the tetrahedra ring TO_4 are present. In the region of the stretching vibrations of the OH groups, two distinct types of vibrational modes can be distinguished: those related to the vibrational modes of the OH groups in the V sites (between 3400 and 3615 cm^{-1}) and those due to the OH groups in the W site (3630-3800 cm^{-1}).

Experimental Techniques

Fifteen tourmaline crystals belonging to the dravite-schorl series were studied in this work (Figure S1 (Supplementary Information)) in order to obtain a correlation between their chemical composition, particularly the relative content of iron and magnesium, and the parameters in the Raman spectrum. The provenances of these minerals are reported in Table 1.

Raman spectra were obtained with a Micro-Raman spectrometer Horiba Jobin-Yvon LabRam equipped with an x-y motorised stage and a confocal Olympus microscope with a 50x ULWD objective, which allows spatial resolution of about 2 μm and a spectral resolution of 2 cm^{-1}. Two

excitation lines were used: a 632.8 nm He-Ne laser for the analysis of the lower wavenumber part of the spectrum (150-750 cm^{-1}) and a 473.1 nm frequency-doubled Nd:YAG laser for the OH region (3400-3800 cm^{-1}). Instrument calibration was done before each measurement session with the 520.7 cm^{-1} mode of silicon for the low-wavenumbers part of the spectrum and with the 2825 cm^{-1} neon emission line for the OH region. The two different excitation lines were used to highlight the two distinct spectral regions: the signal in the OH stretching region is stronger when using a 473.1 nm line than when using a 632.8 nm line, allowing us to precisely analyse the weak ^{W}HO peaks as well. However, fluorescence is higher in the fingerprint region when a higher energy excitation line is used, hence the 632.8 nm line is preferred. Any fluorescence signal in the Raman spectra was subtracted using a polynomial baseline.

Raman measurements with a portable spectrometer were also performed with a RaPort handheld spectrometer by EnSpectr with a 532nm wavelength, a spatial resolution of about 0.5 mm, and a spectral range between 120 and 4000 cm^{-1}, with a spectral resolution of about 8-11 cm^{-1}.

Both analyses with Micro-Raman and portable-Raman were obtained with the same crystal orientation; in particular, we analysed the tourmaline samples with incident light polarised parallel to the crystal c-axis. In this way, we are sure that the relative peak intensities in different samples are not affected by orientation effects. The c-axis orientation in tourmalines is easily discernible because of crystal elongation in this direction and the appearance of stripes on the mineral surface parallel to the c-axis.

In order to examine any potential heterogeneity, 6 to 20 Raman measurements were done on different points of the same sample, and the Raman spectrum parameters were then averaged if no significant differences (standard deviation lower than spectral resolution) were identified on a single sample.

The compositional analyses were done by SEM-EDS (Scanning Electron Microscope coupled with Energy Dispersive System). The tourmaline samples were examined with a SEM-EDS Jeol 6400 Scanning Electron Microscope equipped with an Oxford EDS (Energy Dispersive System) microprobe. Microprobe analysis operating conditions were 20 kV and 1.2 mA current, ~1 µm beam diameter, and 75 s counting time; ~15 analytical points per sample were averaged because no evident chemical zoning was detected in every sample. Some samples were embedded in epoxy resin, polished to make them flat, and covered with a high-conductance thin graphite film to avoid charging effects. Other samples, especially large crystals, were observed “as it is", which is deposited on a tape layer

and covered with graphite. SEM images were obtained using both secondary and back-scattered electron detectors to better assess the presence of composition heterogeneities.

Results and Discussion

For every tourmaline sample, Mg/(Mg+Fe) was calculated from data obtained with SEM-EDS analysis, considering all magnesium and iron detected. In this way, we are considering that all the detected magnesium and iron are located at the Y sites. This strong assumption is possible thanks to the homogeneity of aluminium and silicon content, which we assumed were located in Z and T sites, respectively, and the low concentration of other elements (Ti, Mn, Cu, Cr, Zn, and V) that could be present in Y sites. However, effects related to site disorder can be present, as we will see in the following paragraphs: in fact, Al can be present in Y sites, while Fe and Mg can also be distributed in Z sites [17–20]. From 6 to 20 different points on the same mineral were taken in order to evaluate possible heterogeneities. Compositions in oxide wt% are reported in Table 2. For this work, we calculated from these data the atomic% compositions in order to evaluate the Mg/(Mg+Fe) ratio, verifying the accuracy of the obtained values through the normalisation procedures described in Henry et al. (Appendix 5) [1], *i.e.* normalising the number of oxygen atoms to 24.5 a.p.f.u.; the composition in atomic% of each sample is reported in Table S1 (Supporting Information). In the conversion from oxide wt% to atomic%, since we are not able to precisely determine the iron valence from SEM-EDS measurements, we considered all the iron as ferrous, which is more likely to occupy the Y sites with respect to the ferric iron. SEM-EDS analysis doesn't allow to clearly distinguish between dravite $NaMg_3Al_6(Si_6O_{18})(BO_3)_3(OH)_3OH$ and oxy-dravite $Na(Al_2Mg)Al_6(Si_6O_{18})(BO_3)_3(OH)_3O$; some help in this sense will arrive from Raman spectroscopy, analysing the OH stretching region.

The Raman spectra obtained by micro-Raman on all the tourmaline samples are shown in Figure 1. Their order is given by the Mg/(Mg+Fe) ratio, as obtained from SEM-EDS data; all the samples with Mg/(Mg+Fe)>0.5 are considered dravite, while minerals with Mg/(Mg+Fe)<0.5 are schorl [21,22]. In the following, the different spectral regions will be analysed separately. Then we will compare the micro-Raman results with portable Raman spectra (Figure 4). Mg/(Mg+Fe) ratios and the main Raman spectra parameters obtained for each sample are reported in Table 3. Raman spectrum parameters and SEM-EDS compositions were averaged for each sample because, in some cases, doing Raman and SEM-EDS measurements at the same spot was not possible due to the mineral's non-regular surface. As a result, the values given are the average of each sample.

Schorl is considered a bad Raman scatterer due to its typical black colour, which might induce excessive absorption of incident light; yet, using the same measurement settings as for dravite, we got well-defined spectra for schorl samples as well.

200 – 315 cm^{-1} spectral range

P_1 and P_2 peaks are the main vibrational modes in the 200–315 cm^{-1} spectral range (Figure 1A). The position of peak P_1 (Figure S2 (Supporting Information)) appears to remain stable, approximately at 216 cm^{-1} for Mg/(Mg+Fe) values above 0.5 (dravite). However, for schorl samples below this value, the behaviour of this peak becomes more complex. In some samples, it remains stable around 216 cm^{-1}, similar to dravite, while in other cases, a shift towards approximately 202 cm^{-1} is observed. Although there seems to be a dependence on the Mg/(Mg+Fe) ratio, this bimodal behaviour could be due to the presence of other elements substituting for magnesium and iron in the Y sites. However, none of the other elements that can be present on the Y sites show a correlation with this trend. The main causes could be the presence of lithium, which cannot be detected using SEM-EDS, or the partial substitution of iron-magnesium-aluminium in the Y and Z sites [17–20], although the latter hypothesis is unlikely; only for sample P2 a shift in both parameters is visible when evaluating the behaviour of the P_Z peak (described in the following section) and the peak P_3 positions, as we would predict based on the provided data from Watenphul et al. [14], while other samples reveal no significant differences: the position of the P_3 peak is expected to be approximately 315 cm^{-1}, as showed in Figure S3 (Supplementary Information), and a shift to lower wavenumbers can be attributed to the presence of Fe^{3+} in Y sites. However, the shift in P_3 peak position seen in this study is significantly smaller than the one observed in prior studies for samples with high Fe^{3+} content in Y sites [14]. Also sample T1 shows a shift to lower wavenumber of about 5 cm^{-1} only for P_3 peak, indicating the possible presence of low Fe^{3+} content in Y sites. Furthermore, sample T1 contains a high concentration of quartz impurities, as evidenced by the spectra in Figures 1 and 4, which show the usual quartz peak at 465 cm^{-1}; for these reasons, the composition of sample T1 should be more complex than the one derived by SEM-EDS.

The position of peak P_2 follows a more defined trend, as shown in Figure 2. For dravite samples, there is a linearly dependent shift of P_2 with respect to the Mg/(Mg+Fe) ratio, indicated by the blue line. As the magnesium content increases, the P_2 peak shifts towards higher wavenumbers, reaching approximately 244 cm^{-1}. For Mg/(Mg+Fe) values below 0.5, the position of P_2 is more stable around 237 cm^{-1}, although there is a slight shift towards higher wavenumbers with increasing iron content,

i.e., a decreasing Mg/(Mg+Fe) ratio, represented by the red line in Figure 2. In general, we can observe a distinct difference in the positions of P_2 between dravite and schorl: in the former, the peak is located above 239 cm^{-1}, while in the latter, it is below. Therefore, we can use this value as a threshold to distinguish between the two tourmaline species. The trends of these two lines can provide an estimation of the Mg/(Mg+Fe) ratio, although it may be imprecise.

Also interesting is the behaviour of the saddle point between the peaks P_1 and P_2, which we have named $P_{1/2}$. Its position shifts towards higher wavenumbers as the magnesium content increases, ranging from a minimum of approximately 220 cm^{-1} for schorl to a maximum of 230 cm^{-1} for dravite. However, determining the exact position of this point is challenging because, unlike P_1 and P_2, it does not correspond to a peak in the spectrum but rather to a saddle point (nevertheless, it is necessary to obtain a good spectrum interpolation). Consequently, especially for schorl samples, the error in determining the position is significantly high, as reported in Figure S4 (Supporting Information).

Finally, it is interesting to note the dependence of the relative intensity of the peaks P_1 and P_2 (measured with the same crystal orientation in all the analysed samples) on the composition. As shown in Figure 1A, the intensity of P_1 appears to increase with increasing magnesium content, while P_2 does not show significant variation. By studying this behaviour in detail, the graph in Figure 3 is obtained, where it can be observed that the ratio between the intensity of P_1 and that of P_2 increases linearly with the Mg/(Mg+Fe) ratio. Inverting the linear interpolation, we can obtain the Mg/(Mg+Fe) value with the following formula:

$$Mg/(Mg+Fe) = \frac{I(P_1)/I(P_2) - 0.03}{1.3}$$

Estimating the composition based on these parameters is not very precise: partial overlap of these two peaks, especially in schorl samples, can induce errors in the intensities evaluation of P_1 and P_2; however, the relative intensity can be used to quickly distinguish dravite from schorl in qualitative measurements for *in-situ* analysis: for ratios equal to or greater than 1, it is definitely tourmalines belonging to the first species, while for ratios below 0.4, it is the second species. The relative intensity of P_1 and P_2 peaks was already studied by Watenphul et al. [14], finding an increasing value for this parameter with higher Mg content in Y sites, which agrees with our results on Mg-Fe relative content.

The analysis performed with the portable Raman instrument (Figure 4) on the same samples provided results consistent with those found in the measurements made with micro-Raman for each

parameter in this spectral region (green diamonds in Figures 2, 3, S2 and S4 (Supporting Information)). Consequently, we can state that even *in-situ* measurements with the portable Raman instrument can be sufficient to obtain information about the Mg/(Mg+Fe) ratio in the analysed tourmalines and to recognise dravite and schorl species.

360 – 750 cm^{-1} spectral range

In the spectral region between 360 and 750 cm^{-1}, no vibrational mode is directly correlated to the Y sites and their composition. However, a shift to a lower wavenumber of the P_Z peak (from his typical position at approximately 370 cm^{-1}) can show the presence of Fe^{3+} in the Z site, replacing aluminium, as described by Watenphul et al. [14]. This could explain the bimodal behaviour of the P_1 peak observed earlier, although only the samples P2, with the larger shift of the P_Z peak, exhibit a shift in the P_1 peak, while other samples do not show both of these two features (Figure S5 (Supporting information)). Regarding sample P2, the combination of shifts in both P_1 and P_Z peaks actually indicates the presence of iron in Z sites, as the iron content in Table 2 is much higher than the other samples, together with a lower aluminium content.

There appears to be no association between the composition and the positions of the four peaks detected in the vibrational modes between 600 and 700 cm^{-1} assigned to the TO_4 tetrahedra, which are around 634, 649, 674, and 701 cm^{-1}, respectively.

OH stretching region

In the spectral range of OH stretching, two types of vibrational modes are present: ^{V}OH and ^{W}OH (Figure 1B). To study the former, we relied on the results obtained by Watenphul et al. [16], where the following formula was derived to obtain the concentration (C) of the majority element in the Y site:

$$C(a.p.f.u.) = (3I_{v_{OH_3}} + 2I_{v_{OH_2}} + I_{v_{OH_1}})/I_{v_{OH_{tot}}} \quad (1)$$

$I_{v_{OH_1}}$, $I_{v_{OH_2}}$ and $I_{v_{OH_3}}$ are the intensities of the three peaks used to fit the ^{V}OH band, and, according to Watenphul et al. [16], they are related to the occupation of 3 Y sites and 6 Z sites surrounding the 3 V sites in the unit cell. In particular, $^{V}OH_1$ is related to the $^{Y}C^{Z}Al^{Z}Al$+2 $^{Y}Al^{Z}Al^{Z}Al$ configuration, $^{V}OH_2$ to 2$^{Y}C^{Z}Al^{Z}Al$+ $^{Y}Al^{Z}Al^{Z}Al$ and $^{V}OH_3$ to 3$^{Y}C^{Z}Al^{Z}Al$ where C is the dominant element in the Y site for the analysed tourmaline species. In our case, we considered C=Mg for dravite samples, and the iron content was assumed to be the remaining content in the Y site, i.e., 3-C. Vice versa for schorl samples. In the interpolation of the ^{V}OH band, the positions of the three peaks were fixed

depending on the ratio X=Mg/(Mg+Fe) obtained through SEM-EDS. For X=0 (schorl), the positions are respectively 3500±3, 3545±2, and 3566±1 cm^{-1} for $^{V}OH_1$, $^{V}OH_2$, and $^{V}OH_3$, while for X=1 (dravite), they are found at 3494±8, 3534±7, and 3573±4 cm^{-1} [16]. We then linearly varied the position of the three peaks, depending on X, between the two values of the end members. Subsequently, the X ratio was calculated using the previous formula (1) and compared with the ratio obtained from SEM-EDS measurements. As can be observed in Figure S6 (Supporting Information), the two ratios appear to be similar to each other, confirming the validity of this formula not only for the end members but also for some samples with intermediate compositions between dravite and schorl. The discrepancies from the blue line (one-to-one correspondence) could indicate the presence of aluminium in the Y site, replacing magnesium for the points above the line or iron for the points below it. In the same way, they could also indicate the presence of magnesium or iron replacing aluminium in the Z site. However, the discrepancies are much higher approaching the value Mg/(Mg+Fe) = 0.5; without fixing the three peaks' positions, these differences would have been even greater. Moreover, Watenphul formula considers only aluminium replacing the dominant element in the Y sites, while in the dravite-schorl series, we have both magnesium and iron replacing each other. Therefore, considering these aspects, the assignment of $^{V}OH_1$, $^{V}OH_2$, and $^{V}OH_3$ peaks should be reviewed for the dravite-schorl series, considering the presence of both magnesium and iron in the Y sites influencing the ^{V}OH stretching modes.

Particularly interesting is also the trend of the ^{W}OH peaks that appear in all spectra: $^{W}OH_1$ and $^{W}OH_3$, assigned respectively to $^{Y}(Mg,Fe)^{Y}Al\ ^{Y}Al\text{-}^{X}\square$ and $^{Y}(Mg,Fe)\ ^{Y}(Mg,Fe)^{Y}Al\text{-}^{X}Na$ configurations in dravite and schorl [16]. The position of the first one shows no specific dependence on the Mg/(Mg+Fe) ratio but oscillates around 3630 cm^{-1}.

The shift of the $^{W}OH_3$ peak position towards higher wavenumbers becomes more noticeable as the magnesium content increases, as depicted in Figure 5. As a result, the obtained linear interpolation can be reversed to obtain the following formula, which enables the calculation of the Mg/(Mg+Fe) ratio based on the position of the $^{W}OH_3$ peak:

$$Mg/(Mg+Fe) = \frac{\omega(^{W}\mathrm{OH}_3) - 3717.0}{20}$$

Therefore, this formula can be used to obtain a more precise Mg/(Mg+Fe) ratio compared to the one found using the ratio between the intensities of peaks P_1 and P_2. However, comparing the Mg/(Mg+Fe) ratio obtained by the two different formulas with the Mg/(Mg+Fe) obtained from SEM-EDS measurement on the samples studied in this work, we found out that using both formulas and averaging the resulting values can be useful in obtaining slightly more reliable results.

The total amount of OH is reflected from the intensity of the Raman bands involving ^{W}OH not bound to vacancy sites. In presence of small amount of OH (less than 3.3 a.p.f.u.) [16], the OH groups tend to occupy preferably the sites near the vacancies. The presence of Raman bands in the 3700-3800 cm^{-1} range indicates then a larger amount of OH also in dravite samples, suggesting that our samples are not oxy-dravites.

Regarding the measurements taken with the portable Raman instrument, it was not possible to obtain acceptable results as the signal in the OH stretching spectral range has a low signal-to-noise ratio. This is due to the portable Raman instruments, which typically do not have great efficiency in the OH stretching modes region because they are designed for better performance in the fingerprint region. Furthermore, unlike the 473.1 nm line used in micro-Raman analysis, the excitation line at 532 nm is insufficient to obtain a well-defined signal of the OH group peaks due to the lower intensities of the peaks yielded by a lower energy excitation line, which, combined with the instrument's poor efficiency in the OH region, makes it impossible to detect the weak ^{W}HO modes.

Conclusion

In this work, we found many relations between Mg/(Mg+Fe) and Raman spectra parameters in tourmalines belonging to the dravite-schorl series. Most remarkable are the results obtained for YO_6 and ^{W}HO vibrational modes, which showed linear dependence between the relative intensities of P_1 and P_2 peaks and Mg-Fe relative content, as well as the dependence of the $^{W}OH_3$ peak position on this composition ratio, finding two different formulas to calculate the Mg/(Mg+Fe) ratio from these Raman parameters. We also discovered that the P_2 peak position value of 239 cm^{-1} can be used as a threshold to discriminate between dravite and schorl.

Moreover, we evaluated the validity of the Watenphul et al. [16] formula for the calculation of Y site composition from ^{V}OH peaks relative intensities. This formula is dependable not only for end members but also for some samples with intermediate composition in the dravite-schorl series and could possibly bring information on Z-Y site disorder, but a reassignment of $^{V}OH_1$, $^{V}OH_2$, and $^{V}OH_3$ peaks should be done considering both Mg and Fe in the Y sites.

In conclusion, we proved that all these results can be obtained with a portable Raman used for *in-situ* analysis, at least in the fingerprint region. Also, the OH stretching region could be studied with an adequate signal-to-noise ratio.

References

[1] D. J. Henry, M. Novák, F. C. Hawthorne, A. Ertl, B. L. Dutrow, P. Uher, F. Pezzotta, *American Mineralogist* **2011**, *96*, 895.

[2] F. C. Hawthorne, *The Canadian Mineralogist* **2002**, *40*, 789.

[3] B. L. Dutrow, D. J. Henry, *Elements* **2011**, *7*, 301.

[4] V. J. Van Hinsberg, D. J. Henry, B. L. Dutrow, *Elements* **2011**, *7*, 327.

[5] L. S. Brown, *Am Mineral* **1929**, *14*, 238.

[6] G. Von Goerne, G. Franz, J.-L. Robert, *The Canadian Mineralogist* **1999**, *37*, 1025.

[7] D. J. Henry, B. L. Dutrow, *Journal of Geosciences (Czech Republic)* **2018**, *63*, 77.

[8] S. Andò, E. Garzanti, *Geological Society, London, Special Publications* **2014**, *386*, 395.

[9] D. J. Henry, C. V Guidotti, *American Mineralogist* **1985**, *70*, 1.

[10] D. J. Henry, B. L. Dutrow, in *Boron - Mineralogy, Petrology, and Geochemistry*, De Gruyter, **1996**, vol. 33, pp. 503–558.

[11] K. Bónová, M. Jafarzadeh, J. Bóna, T. Mikuš, J. Anjerdi, A. Najafzadeh, R. Mahari, *J Asian Earth Sci* **2021**, *221*, 104943.

[12] V. J. Van Hinsberg, J. C. Schumacher, *Can Mineral* **2011**, *49*, 177.

[13] V. J. Van Hinsberg, D. J. Henry, H. R. Marschall, *Can Mineral* **2011**, *49*, 1.

[14] A. Watenphul, J. Schlüter, F. Bosi, H. Skogby, T. Malcherek, B. Mihailova, *American Mineralogist* **2016**, *101*, 2554.

[15] B. Gasharova, B. Mihailova, L. Konstantinov, *Eur. J. Mineral* **1997**, *9*, 935.

[16] A. Watenphul, M. Burgdorf, J. Schlüter, I. Horn, T. Malcherek, B. Mihailova, *American Mineralogist* **2016**, *101*, 970.

[17] F. Bosi, *Can Mineral* **2011**, *49*, 17.

[18] F. Bosi, G. B. Andreozzi, U. Hålenius, H. Skogby, *Mineral Mag* **2015**, *79*, 515.

[19] F. C. Hawthorne, D. J. MacDonald, P. C. Burns, *American Mineralogist* **1993**, *78*, 265.

[20] F. Bosi, S. Lucchesi, *European Journal of Mineralogy* **2004**, *16*, 335.

[21] F. Bosi, C. Biagioni, R. Oberti, *Minerals* , DOI:10.3390/min9100591.

[22] F. Bosi, F. Hatert, U. Hålenius, M. Pasero, R. Miyawaki, S. J. Mills, *Mineral Mag* **2019**, *83*, 627.

***Table 1**: Provenance of the analysed tourmaline samples.*

Sample	Provenance	Species	Dimensions (mm)
B1	Brazil	Dravite	5x5x19
E1	Grotta d'Oggi, Elba, Italy	Schorl	2x2x4
E2	Grotta d'Oggi, Elba, Italy	Schorl	1x5x8
E3	Grotta d'Oggi, Elba, Italy	Schorl	1x2x8
E4	Grotta d'Oggi, Elba, Italy	Schorl	1x2x4
L1	Val Bodengo, Sondrio, Lombard Alps, Italy	Dravite	6x6x7
L2	Piona, Lecco, Lombard Alps, Italy	Dravite	10x10x20
L3	Piona, Lecco, Lombard Alps, Italy	Schorl	12x12x15
L4	Piona, Lecco, Lombard Alps, Italy	Schorl	7x7x20
L6	Val Bodengo, Sondrio, Lombard Alps, Italy	Dravite	10x13x16
P1	Ornavasso, Verbano-Cusio-Ossola, Piedmontese Alps, Italy	Dravite	3x4x12
P2	Ca' dei Pescatori, Biella, Piedmontese Alps, Italy	Schorl	1x1x3
P3	Ban Est, Verbano-Cusio-Ossola, Piedmontese Alps, Italy	Dravite	1x1x2
P4	Pizzo Marcio, Verbano-Cusio-Ossola, Piedmontese Alps, Italy	Schorl	1x2x2
T1	Fornovolasco, Lucca, Tuscany, Italy	Schorl	2x20x12

355

***Table 2**: Sample composition in oxide wt% obtained by SEM-EDS measurement.*

Sample	Na_2O	MgO	Al_2O_3	SiO_2	K_2O	CaO	TiO_2	V_2O_3	Cr_2O_3	MnO	FeO	CuO	ZnO
B1	1.5±0.1	9.4±0.4	35.6±0.1	45.2±0.3	0.1±0.1	1.5±0.2	1.3±0.1	0	0	0.1±0.1	5.1±0.8	0	0.2±0.2
E1	1.7±0.2	1.5±0.1	34.5±0.4	41.6±0.8	0.1±0.1	0.4±0.1	0.8±0.1	0	0	0.6±0.1	19±1	0	0.2±0.1
E2	1.6±0.2	3.9±0.2	34.4±0.2	42.6±0.2	0.1±0.1	0.5±0.1	1.0±0.1	0	0	0.3±0.1	15.5±0.2	0.1±0.1	0
E3	1.4±0.1	4.2±0.2	36.2±0.6	42.4±0.3	0	0.5±0.1	0.7±0.2	0	0	0.1±0.1	14.4±0.3	0	0.1±0.1
E4	1.7±0.3	3.1±0.2	35.6±0.3	42.9±0.7	0.1±0.1	0.2±0.08	0.6±0.1	0	0	0.4±0.1	15.3±0.9	0	0.1±0.1
L1	1.5±0.1	6.7±0.2	36.2±0.5	44.1±0.4	0	1.1±0.1	1.1±0.2	0.1±0.1	0	0.1±0.1	8.9±0.3	0.1±0.1	0.1±0.1
L2	1.9±0.1	5.0±0.2	39.2±0.4	45.7±0.3	0.2±0.1	0.5±0.1	0.5±0.1	0	0	0.1±0.1	6.9±0.5	0	0
L3	1.0±0.1	4.6±0.2	36±0.1	41.2±0.6	0.1±0.1	0.4±0.1	0.9±0.1	0	0.1±0.1	0.2±0.1	15.4±0.7	0	0.1±0.1
L4	1.3±0.1	3.1±0.1	35.4±0.1	41.0±0.3	0.1±0.1	0.1±0.1	0.6±0.1	0	0	0.3±0.1	18.1±0.3	0	0
L6	1.5±0.1	7.3±0.3	36.1±0.3	44.3±0.5	0.2±0.1	1.5±0.2	1.1±0.1	0.2±0.1	0.1±0.1	0	7.7±0.6	0	0
P1	2.0±0.1	7.7±0.1	34.7±0.8	43±2	0	0.4±0.1	1.1±0.1	0.1±0.1	0	0.3±0.1	11±3	0.2±0.1	0.1±0.1
P2	1.5±0.1	6.9±0.4	26.9±0.8	40.4±0.7	0.1±0.1	2.1±0.5	0.8±0.4	0.1±0.2	0	0.1±0.1	21±1	0.1±0.1	0
P3	1.8±0.1	10.5±0.2	36.7±0.5	46.7±0.2	0.1±0.1	1.3±0.2	0.7±0.1	0	0.1±0.1	0	2.0±0.2	0	0.1±0.2
P4	1.5±0.1	5.2±0.1	34.1±0.3	42±1	0.2±0.1	0.5±0.1	0.1±0.1	0	0	0.3±0.1	16±1	0	0
T1	1.0±0.1	6.6±0.2	32.5±0.2	42.0±0.1	0.1±0.1	2.3±0.2	2.3±0.1	0	0	0.1±0.1	13.1±0.2	0	0

360

365

Table 3: Mg/(Mg+Fe) ratio and main Raman spectra parameters for each sample.

Sample	Mg/(Mg+Fe)	P_1	$P_{1/2}$	P_2	P_Z	$^{W}OH_3$	$I(P_1)/I(P_2)$
B1	0.77±0.08	215.6±0.2	228.9±0.9	243.1±0.1	369.8±0.1	3732.9±0.7	1.1±0.1
E1	0.13±0.01	202.7±0.7	222±2	237.5±0.3	366.5±0.5	3719.9±0.5	0.30±0.05
E2	0.31±0.01	216±3	225±7	237±2	364.0±0.2	3725±1	0.16±0.05
E3	0.33±0.01	216±2	224±3	237±1	366±1	3725±2	0.7±0.2
E4	0.26±0.03	205±1	2224±2	237.8±0.4	366.4±0.5	3718.5±0.8	0.28±0.05
L1	0.57±0.01	213.9±0.4	226.6±0.9	240.5±0.2	368.6±0.2	3729.0±0.4	0.68±0.04
L2	0.56±0.12	217±2	2273±4	239.5±0.8	368.1±0.4	3728.7±0.8	0.7±0.1
L3	0.34±0.02	215±2	227±2	238.5±0.8	367.3±0.3	3724±4	0.7±0.1
L4	0.23±0.01	211.3±2	224±2	237.1±0.6	366.1±0.1	3720±1	0.5±0.1
L6	0.63±0.05	214.6±0.9	2278±2	241.2±0.4	368.5±0.1	3730±1	0.8±0.1
P1	0.56±0.13	215±1	227±2	242.8±0.8	370.1±0.8	3735±2	1.00±0.08
P2	0.37±0.08	209±1	224.2±0.9	237.3±0.5	361.7±0.7	3722±4	0.57±0.05
P3	0.91±0.07	216.8±0.3	229.5±0.7	243.8±0.4	370.2±0.3	3734.1±0.7	1.3±0.1
P4	0.36±0.03	215±2	223.0±0.7	236.5±0.4	365.3±0.2	3722±1	0.52±0.06
T1	0.47±0.04	215±2	222±3	236.4±0.6	364.5±0.5	3728±1	0.9±0.1

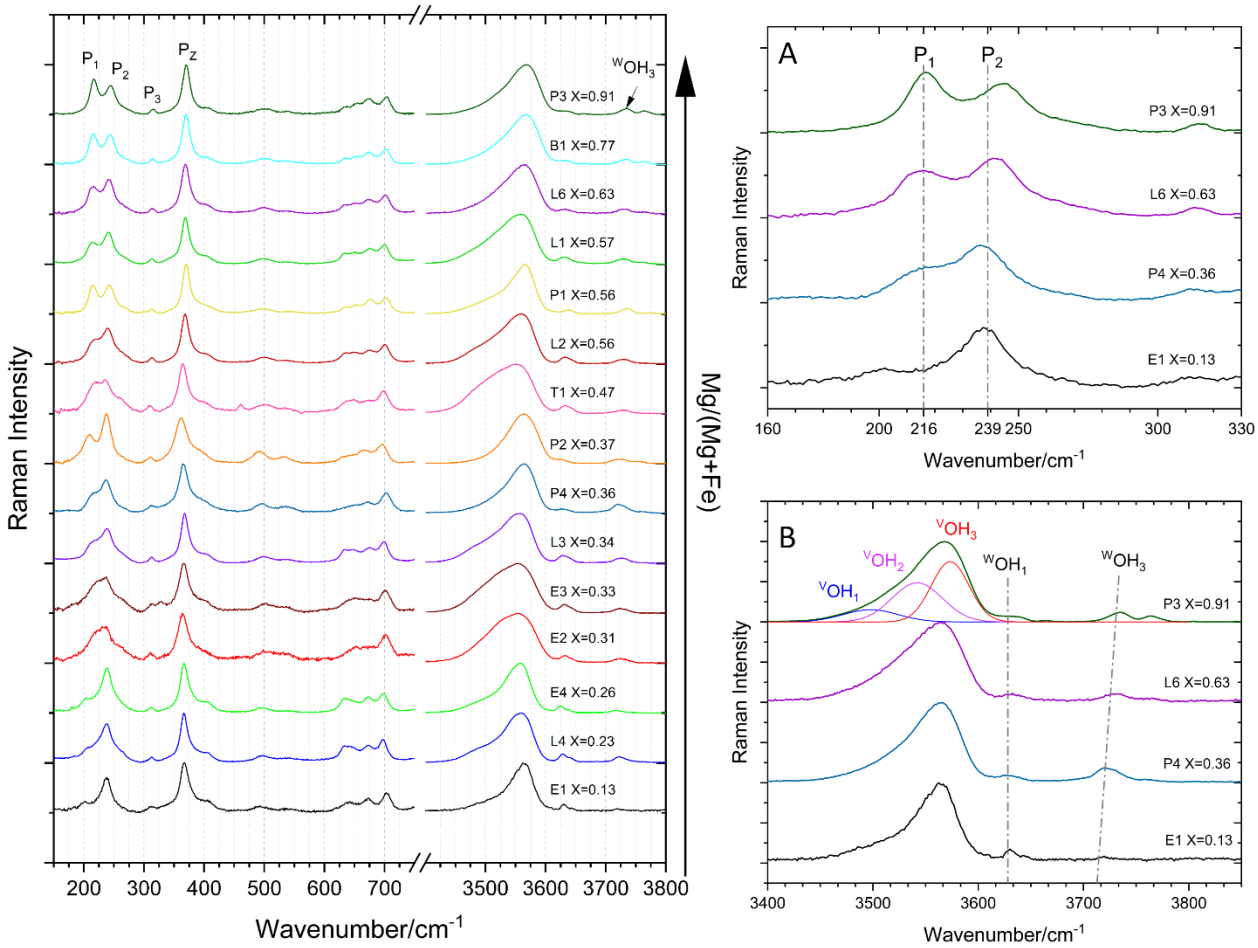

Figure 1: Raman spectra of the analysed samples obtained with the micro-Raman spectrometer. Mg content is higher in spectra at the top (dravite), while Fe has a higher concentration in samples at the bottom (schorl). For each sample, spectra in the fingerprint region (from 150 to 750 cm^{-1}) and in the OH stretching region are presented. The X value shown on each spectrum represents the Mg/(Mg+Fe) ratio for that sample. The principal peaks investigated in this paper are highlighted in the first spectrum. In Figure 1A, the region between 200-330 cm^{-1} is highlighted together with the positions of the P_1 and P_2 peaks. In Figure 2B, the OH stretching region is represented, with the $^{V}OH_1$, $^{V}OH_2$, $^{V}OH_3$, $^{W}OH_1$ and $^{W}OH_3$ peak positions indicated.

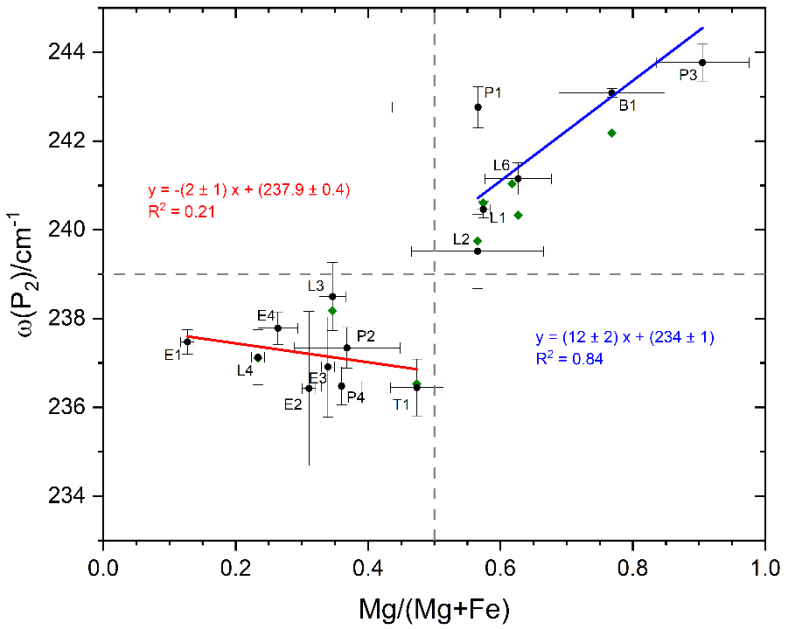

Figure 2: P_2 position depending on the Mg/(Mg+Fe) ratio. Black dots represent micro-Raman data, interpolated by a blue line (dravite samples) and a red line (schorl samples). Green diamonds are the portable Raman data obtained on the same samples.

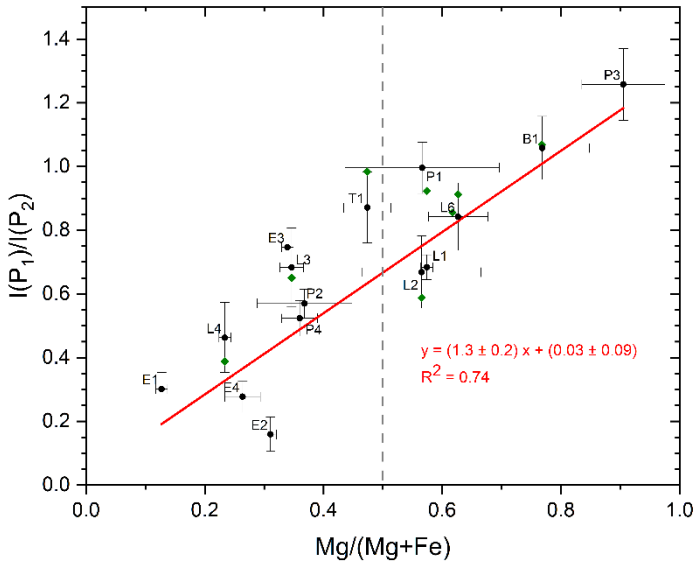

385

Figure 3: P_1-P_2 intensity ratio depending on the Mg/(Mg+Fe). Black dots represent micro-Raman data, interpolated by the red line. Green diamonds are the portable Raman data obtained on the same samples.

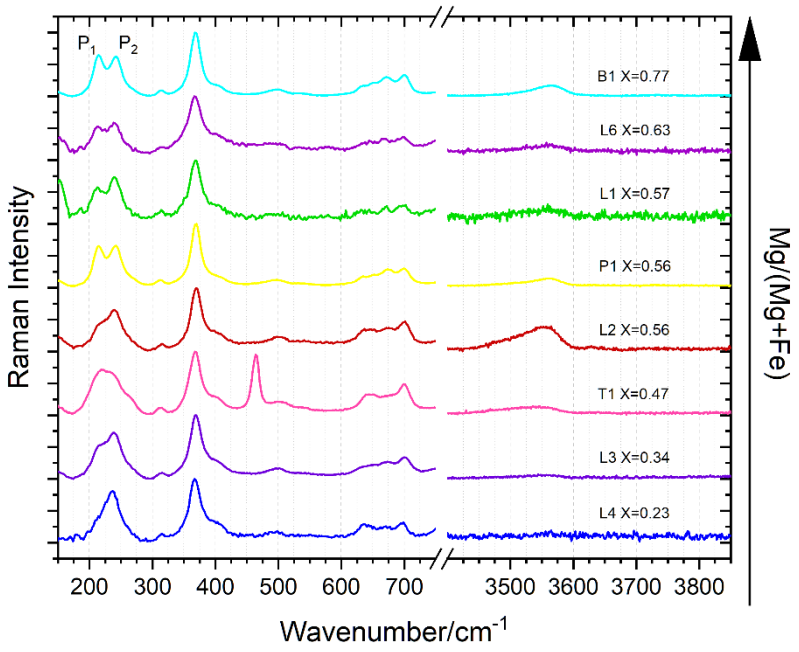

390 **Figure 4:** Raman spectra of the analysed samples obtained with the portable-Raman spectrometer. Mg content is higher in spectra at the top (dravite), while Fe has a higher concentration in samples at the bottom (schorl). For each sample, spectra in the fingerprint region (from 150 to 750 cm^{-1}) and in the OH stretching region are presented. The X value shown on each spectrum represents the Mg/(Mg+Fe) ratio for that sample.

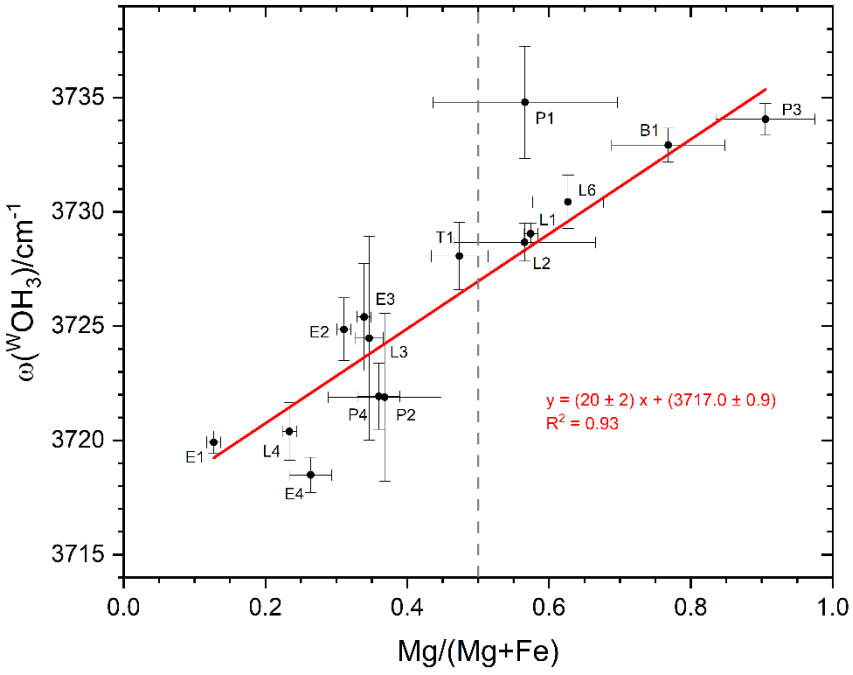

395 **Figure 5:** $^{W}OH_3$ position depending on the Mg/(Mg+Fe) ratio. Black dots represent micro-Raman data, interpolated by the red line.

Supplementary materials

***Table S1**: Sample composition in atomic% obtained by SEM-EDS measurement.*

	O	Na	Mg	Al	Si	K	Ca	Ti	V	Cr	Mn	Fe	Cu	Zn
B1	61±2	1.01±0.09	4.9±0.3	14.6±0.4	15.7±0.5	0.04±0.02	0.56±0.09	0.34±0.05	0	0	0.03±0.01	1.5±0.3	0	0.05±0.06
E1	61±3	1.2±0.2	0.82±0.07	15±0.6	15.3±0.8	0.05±0.06	0.16±0.02	0.22±0.03	0	0	0.19±0.01	5.7±0.6	0	0.05±0.02
E2	61±2	1.1±0.2	2.1±0.1	14.7±0.3	15.5±0.3	0.05±0.02	0.19±0.03	0.27±0.04	0	0	0.09±0.03	4.7±0.1	0.03±0.03	0
E3	61±2	1±0.1	2.3±0.2	15.4±0.6	15.3±0.4	0	0.19±0.05	0.19±0.05	0	0	0.03±0.02	4.3±0.2	0	0.03±0.02
E4	61±3	1.2±0.2	1.7±0.2	15.2±0.6	15.5±0.7	0.05±0.02	0.08±0.03	0.16±0.02	0	0	0.12±0.03	4.6±0.4	0	0.03±0.04
L1	61±2	1±0.1	3.5±0.2	15±0.5	15.5±0.5	0	0.42±0.05	0.29±0.06	0.03±0.02	0	0.03±0.02	2.6±0.1	0.03±0.01	0.03±0.02
L2	62±2	1.28±0.07	2.6±0.1	16.1±0.5	15.9±0.4	0.09±0.04	0.19±0.02	0.13±0.03	0	0	0.03±0.01	2±0.2	0	0
L3	61±3	0.7±0.09	2.5±0.2	15.4±0.4	14.9±0.6	0.05±0.01	0.16±0.04	0.25±0.04	0	0.03±0.02	0.06±0.01	4.7±0.3	0	0.03±0.04
L4	61±2	0.92±0.07	1.69±0.06	15.3±0.3	15±0.3	0.05±0.02	0.04±0.01	0.17±0.04	0	0	0.09±0.03	5.5±0.2	0	0
L6	61±3	1±0.1	3.8±0.2	14.9±0.5	15.5±0.5	0.09±0.03	0.56±0.07	0.29±0.04	0.06±0.02	0.03±0.02	0	2.3±0.2	0	0
P1	61±7	1.4±0.2	4.1±0.3	15±1	15±2	0	0.15±0.02	0.29±0.04	0.03±0.01	0	0.09±0.04	3±1	0.05±0.01	0.03±0.01
P2	60±5	1.1±0.1	3.8±0.4	11.9±0.9	15±1	0.05±0.02	0.8±0.2	0.2±0.1	0.03±0.06	0	0.03±0.02	6.6±0.7	0.03±0.04	0
P3	61±2	1.2±0.1	5.3±0.2	14.8±0.5	15.9±0.4	0.04±0.02	0.48±0.07	0.18±0.04	0	0.03±0.02	0	0.57±0.07	0	0.03±0.04
P4	61±4	1.06±0.05	2.8±0.1	14.6±0.6	15.2±0.9	0.09±0.04	0.19±0.01	0.03±0.02	0	0	0.09±0.04	5±0.6	0	0
T1	61±2	0.7±0.08	3.6±0.2	13.8±0.4	15.2±0.3	0.05±0.05	0.89±0.09	0.63±0.04	0	0	0.03±0.01	4±0.1	0	0

400

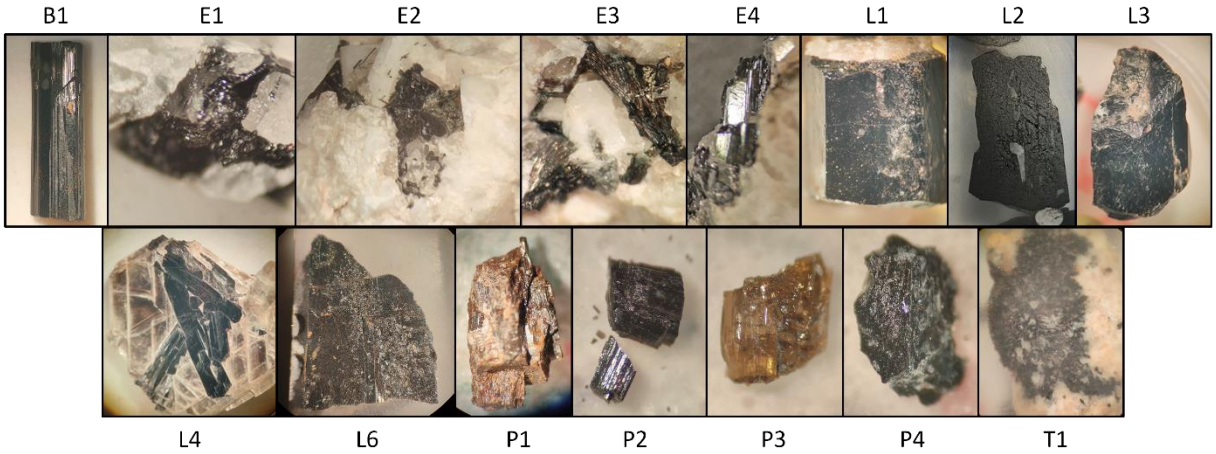

Figure S1: *Images of the fifteen samples analysed in this work.*

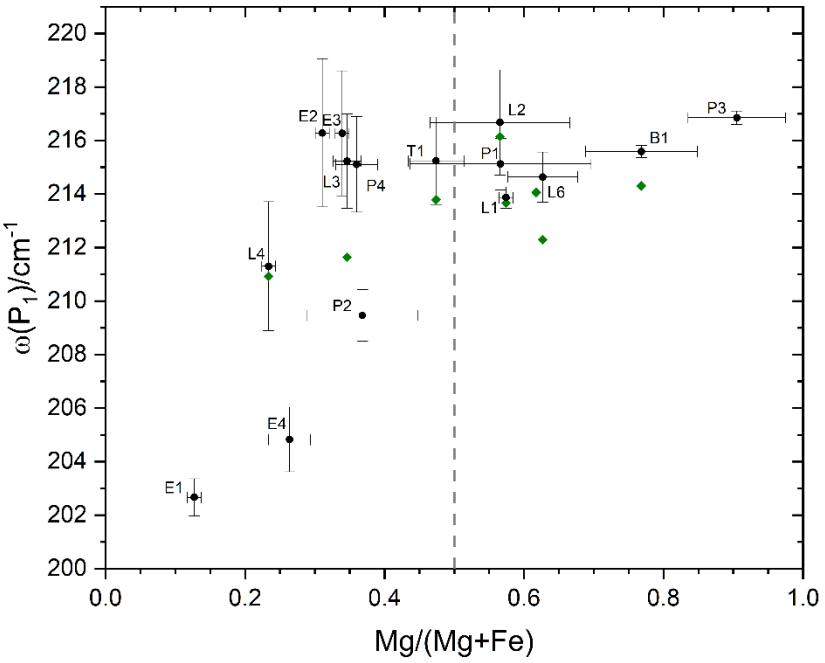

405 **Figure S2:** P_1 position depending on the Mg/(Mg+Fe) ratio. Black dots represent micro-Raman data, while green diamonds are the portable Raman data obtained on the same samples.

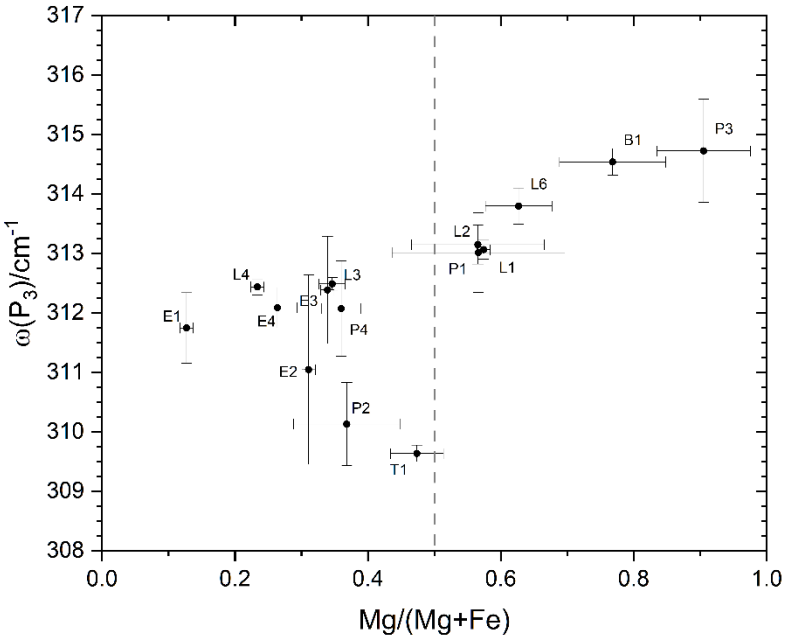

Figure S3: P_3 position depending on the Mg/(Mg+Fe) ratio. Only samples P2 and T1 show a clear shift to lower wavenumbers.

410

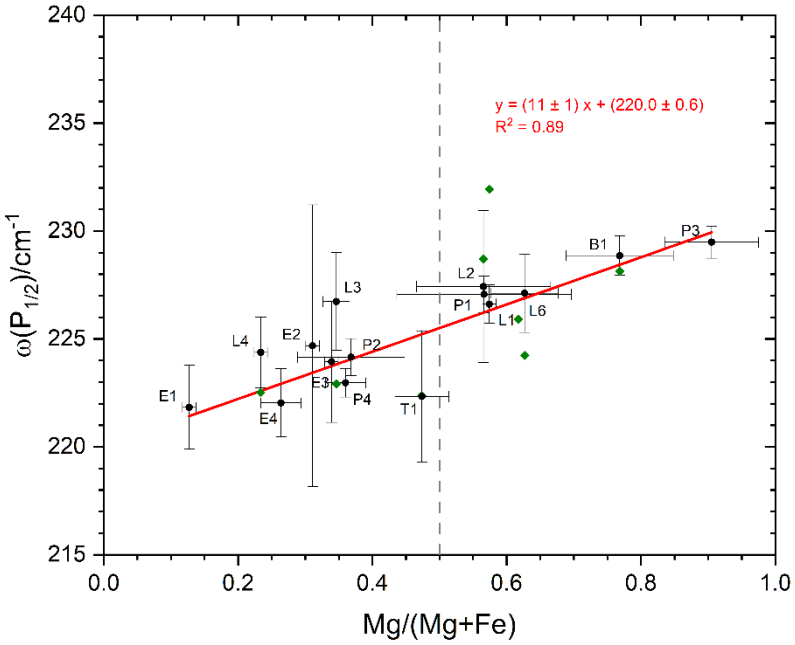

Figure S4: $P_{1/2}$ position depending on the Mg/(Mg+Fe) ratio. Black dots represent micro-Raman data, interpolated by the red line. Green diamonds are the portable Raman data obtained on the same samples.

415

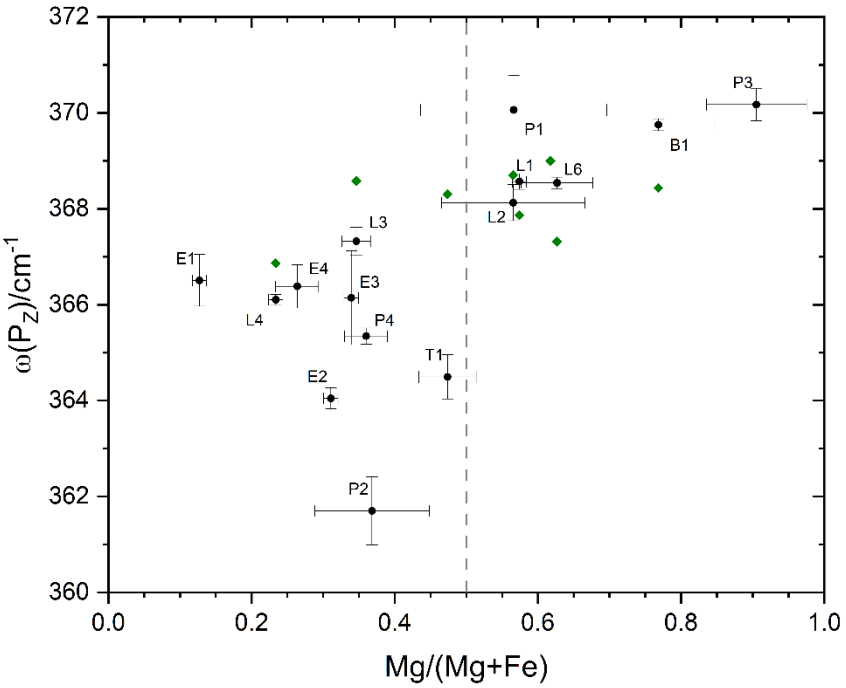

Figure S5: P_Z position depending on the Mg/(Mg+Fe) ratio. Black dots represent micro-Raman data, while green diamonds are the portable Raman data obtained on the same samples.

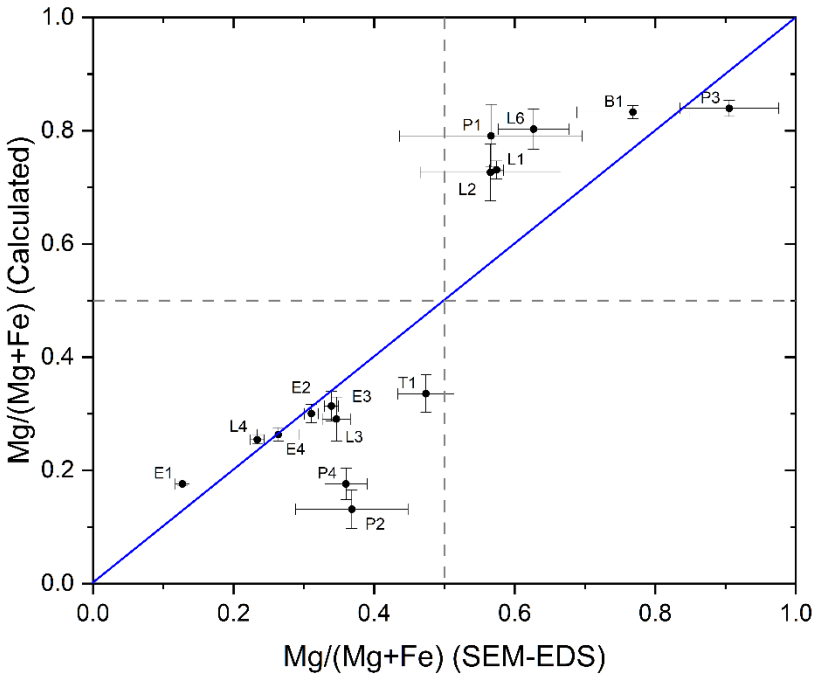

Figure S6: Comparison between the Mg/(Mg+Fe) ratio calculated with formula (1) and measured with SEM-EDS; the blue line represents the one-to-one correspondence between the two ratios.